Open access • Proceedings Article • DOI:10.33012/2016.14845

Intelligent Urban Positioning using Shadow Matching and GNSS Ranging aided by 3D Mapping — Source link

Mounir Adjrad, Paul D. Groves

Published on: 16 Sep 2016

Topics: Ranging, GNSS applications and Pseudorange

Intelligent Urban Positioning using Shadow Matching and GNSS Ranging aided by 3D Mapping

Mounir Adjrad, Paul D Groves
University College London

BIOGRAPHY

Dr Mounir Adjrad is a Postdoctoral Research Associate at University College London (UCL). His current research interests are on Intelligent Urban Positioning (IUP) exploiting conventional GNSS technology augmented by 3D models of urban environments. He has multidisciplinary research experience in industry and academic institutions working on topics such as ultra-wideband technology, GNSS, satellite engineering, radar, biomedical engineering and transport engineering He holds a State Engineering degree in electronics, Magister in signal and communication, and State Doctorate in signal and systems from Ecole Nationale Polytechnique d'Alger, Algeria. (mounir.adjrad@ucl.ac.uk)

Dr Paul Groves is a Senior Lecturer (associate professor) at UCL, where he leads a program of research into robust positioning and navigation within the Space Geodesy and Navigation Laboratory (SGNL). He joined in 2009, after 12 years of navigation systems research at DERA and QinetiQ. He is interested in all aspects of navigation and positioning, including improving GNSS performance under challenging reception conditions, advanced multisensor integrated navigation, and novel positioning techniques. He is an author of more than 80 technical publications, including the book *Principles of GNSS, Inertial and Multi-Sensor Integrated Navigation Systems*, now in its second edition. He holds a bachelor's degree and doctorate in physics. (p.groves@ucl.ac.uk)

ABSTRACT

Conventional GNSS positioning in dense urban areas can exhibit errors of tens of meters due to blockage and reflection of signals by the surrounding buildings. Here, we present a full implementation of the intelligent urban positioning (IUP) 3D-mapping-aided (3DMA) GNSS concept. This combines conventional ranging-based GNSS positioning enhanced by 3D mapping with the GNSS shadow-matching technique. Shadow matching determines position by comparing the measured signal availability with that predicted over a grid of candidate positions using 3D mapping. Thus, IUP uses both pseudo-range and signal-to-noise measurements to determine position. All algorithms incorporate terrain-height aiding and use measurements from a single epoch in time.

Two different 3DMA ranging algorithms are presented, one based on least-squares estimation and the other based on computing the likelihoods of a grid of candidate position hypotheses. The likelihood-based ranging algorithm uses the same candidate position hypotheses as shadow matching and makes different assumptions about which signals are direct line-of-sight (LOS) and non-line-of-sight (NLOS) at each candidate position. Two different methods for integrating likelihood-based 3DMA ranging with shadow matching are also compared. In the position-domain approach, separate ranging and shadow-matching position solutions are computed, then averaged using direction-dependent weighting. In the hypothesis-domain approach, the candidate position scores from the ranging and shadow matching algorithms are combined prior to extracting a joint position solution.

Test data was recorded using a u-blox EVK M8T consumer-grade GNSS receiver and a HTC Nexus 9 tablet at 28 locations across two districts of London. The City of London is a traditional dense urban environment, while Canary Wharf is a modern environment. The Nexus 9 tablet data was recorded using the Android Nougat GNSS receiver interface and is representative of future smartphones. Best results were obtained using the likelihood-based 3DMA ranging algorithm and hypothesis-based integration with shadow matching. With the u-blox receiver, the single-epoch RMS horizontal (i.e., 2D) error across all sites was 4.0 m, compared to 28.2 m for conventional positioning, a factor of 7.1 improvement. Using the Nexus tablet, the intelligent urban positioning RMS error was 7.0 m, compared to 32.7 m for conventional GNSS positioning, a factor of 4.7 improvement.

An analysis of processing and data requirements shows that intelligent urban positioning is practical to implement in real-time on a mobile device or a server.

1. INTRODUCTION

The positioning performance of global navigation satellite systems (GNSS) in dense urban areas is poor because buildings block, reflect and diffract the signals. If the real-time position accuracy using low-cost equipment could be improved to 5m or better, a host of potential applications would benefit. These include situation awareness of emergency, security and military personnel and vehicles; emergency caller location; mobile mapping; tracking vulnerable people and valuable assets; intelligent mobility; location-based services; location-based charging; augmented reality; and enforcement of curfews, restraining orders and other court orders. A further accuracy improvement to around 2m would also enable navigation for the visually impaired; lane-level road positioning for intelligent transportation systems; aerial surveillance for law enforcement, emergency management, building management and newsgathering; and advanced rail signaling.

Buildings and other obstacles degrade GNSS positioning in three ways. Firstly, where signals are completely blocked, they are simply unavailable for positioning, degrading the signal geometry. Secondly, where the direct signal is blocked (or severely attenuated), but the signal is received via a (much stronger) reflected path, this is known as non-line-of-sight (NLOS) reception. NLOS signals exhibit positive ranging errors corresponding to the path delay (the difference between the reflected and direct paths). These are typically a few tens of meters in dense urban areas, but can be much larger if a signal is reflected by a distant building. Thirdly, where both direct line-of-sight (LOS) and reflected signals are received, multipath interference occurs. This can lead to both positive and negative ranging errors, the magnitude of which depends on the signal and receiver designs. NLOS reception and multipath interference are often grouped together and referred to simply as "multipath". However, to do so is highly misleading as the two phenomena have different characteristics and can require different mitigation techniques [1].

There are many different approaches to multipath and NLOS mitigation [2]. A good GNSS antenna is more sensitive to right-hand circularly polarized (RHCP) signals than to left-hand circularly polarized (LHCP) signals. As direct LOS signals are RHCP while most reflected signals are LHCP or mixed polarization, this reduces multipath errors by attenuating the reflected signal components with respect to the direct. Furthermore, NLOS reception can usually be detected from the signal to noise ratio (SNR) measurements, enabling NLOS signals to be eliminated from the position calculation. However, cheaper antennas offer less polarization discrimination and smartphone antennas none at all.

Much of the literature on multipath mitigation is dominated by receiver-based signal-processing techniques [3]. However, because they work by separating out the direct and reflected signals within the receiver, they can only be used to mitigate multipath; they have no effect on NLOS reception at all. Consistency checking selects the most consistent subset of the signals received to compute a position solution from. This is based on the principle that measurements from "clean" direct LOS signals produce a more consistent navigation solution than those from NLOS and severely multipath-contaminated signals. In dense urban areas, a subset comparison approach is more robust that conventional sequential testing [4].

Over the past six years, there has been a lot of interest in 3D-mapping-aided (3DMA) GNSS, a range of different techniques that use 3D mapping data to improve GNSS positioning accuracy in dense urban areas. The simplest form of 3DMA GNSS is terrain height aiding. For most land applications, the antenna is at a known height above the terrain. By using a digital terrain model (DTM), also known as a digital elevation model (DEM), the position solution may be constrained to a surface. In conventional least-squares positioning, this is done by generating a virtual ranging measurement [5]. By effectively removing a dimension from the position solution, this improves the accuracy of the remaining dimensions. In open areas, terrain height aiding only improves the vertical position solution (as one might expect). However, in dense urban areas where the signal geometry is poor, it can improve the horizontal accuracy by almost a factor of two [6].

3D models of the buildings can be used to predict which signals are blocked and which are directly visible at any location [7][8]. This can be computationally intensive. However, the real-time computational load can be reduced dramatically by using building boundaries [9]. These describe the minimum elevation above which satellite signals can be received at a series of azimuths and are precomputed for each candidate position. A signal can then be classified as LOS or NLOS simply by comparing the satellite elevation with that of the building boundary at the corresponding azimuth.

The shadow-matching technique [10] determines position by comparing the measured signal availability and strength with predictions made using a 3D city model over a range of candidate positions. Several research groups have demonstrated this experimentally, using both single and multiple epochs of GNSS data [11][12][13][14][15][16][17][18]. Cross-street position accuracies of a few meters have been achieved in dense urban areas, enabling users to determine which side of the street they're on. This complements GNSS ranging, which is more accurate in the along-street direction in these environments because more direct LOS signals are received along the street than across it. Shadow matching has also been demonstrated in real time on an Android smartphone [19]. A review of shadow matching, including its error sources and how it could be developed further may be found in [20].

3D models of the buildings can also be used to aid conventional ranging-based GNSS positioning. Where the

user position is already approximately known, it is straightforward to use a 3D city model to predict the NLOS signals and eliminate them from the position solution [21][22][23]. However, for most urban positioning applications there is significant position uncertainty. One solution is to define a search area centered on the conventional GNSS position solution and compute the proportion of candidate positions at which each signal is receivable via direct LOS. This can then be used to re-weight a least-squares position solution and aid consistency checking [6]. More sophisticated approaches which score position hypotheses using the GNSS pseudo-range measurements and satellite visibility predictions at each candidate position are presented in [24] and in Section 2.2 of this paper.

Several groups have extended 3D-mapping-aided GNSS ranging by using the 3D city model to predict the path delay of the NLOS signals across an array of candidate positions [25][26][27][28]. A single-epoch positioning accuracy of 4m has been reported [27]. However, unless the search area is small, this approach is very computationally intensive as the path delay cannot easily be pre-computed. The urban trench approach presented in [29] enables the path delays of NLOS signals to be computed very efficiently, but only if the building layout is highly symmetric, so it can only be used in suitable environments. Therefore, NLOS path delay predictions are not used in the work presented here.

3DMA GNSS ranging has also been combined with 'direct positioning' which uses the receiver correlator outputs to score an array of position hypothesis [30].

Clearly, to get the best performance out of GNSS aided by 3D mapping, as much information as possible should be used. Thus, both pseudo-range and SNR measurements from a multi-constellation GNSS receiver should be used, together with both LOS/NLOS predictions and terrain height from 3D mapping. This concept is known as intelligent urban positioning (IUP) [31].

A preliminary implementation of the IUP concept is presented in [32]. This integrates shadow matching with a 3DMA least-squares GNSS ranging algorithm incorporating terrain height aiding, consistency checking, and weighting of the pseudo-ranges according to the average predicted satellite visibility over a search area. Position-domain integration is used with two different weighting approaches. Error covariance-based weighting was found to perform slightly better than weighting using the street azimuth. The overall root mean square (RMS) horizontal (i.e., 2D) single-epoch position accuracy obtained using a u-blox EVK M8T receiver was 6.1 m, compared to 25.9 m using conventional GNSS positioning, a factor of four improvement.

This paper extends this work, incorporating:

- A 3DMA GNSS ranging algorithm based on computing the likelihood of an array of candidate position hypotheses based on the satellite visibility predictions at each position (the least-squares algorithm is retained for initialization);
- Hypothesis-domain integration of 3DMA ranging with shadow matching;
- Additional test sites in the Canary Wharf area of London, which is similar to modern urban environments in North America and Asia;
- Test results using a Nexus 9 tablet equipped with the Android Nougat GNSS receiver interface that will enable 3DMA GNSS ranging to be implemented on a smartphone.

All results presented here are based on a single epoch of GNSS measurements, which suits many location-based service (LBS) applications that require a quick one-time fix. 3DMA GNSS is particularly important for single-epoch positioning because other augmentations, such as carrier-smoothing, carrier-phase positioning and integration with inertial sensors, only work with multiple epochs of GNSS data [2].

An alternative implementation of the intelligent urban positioning concept is presented in [24]. The shadow-matching algorithm is simpler than that used here. A different likelihood-based 3DMA GNSS ranging algorithm is also implemented which uses only the signals predicted to be direct LOS at each candidate position. The experimental tests demonstrate that the method works well. However, as the results presented combine measurements from multiple epochs, they are not directly comparable with the single-epoch results presented here.

Extending the IUP implementation presented here to multiple epochs for navigation and tracking applications is a subject for future work. Better performance can be expected as several researchers have already demonstrated that filtering can improve 3DMA GNSS performance [17][18][24]. Conventional GNSS positioning also works much better with multiple epochs of data. With an extended Kalman filter (within which carrier-smoothing is normally inherent), it is much easier to detect outliers due to NLOS reception and severe multipath interference than it is using single-epoch least-squares positioning. However, 3DMA GNSS also has an important role to play in multi-epoch positioning as it will enable carrier-smoothed, inertially aided and potentially even real-time kinematic (RTK) carrier-phase positioning to be accurately initialized and re-initialized in challenging urban environments.

Section 2 summarizes the positioning algorithms, including the least-squares and likelihood-based 3DMA ranging algorithms, the shadow matching algorithm and the integration algorithms. Section 3 presents experimental test results from data collected using a u-blox EVK M8T consumer-grade GNSS receiver and a Nexus 9 tablet at 28 locations across two districts of London. Section 4 then discusses the practicality of real-time implementation of intelligent urban positioning.

Finally, Sections 5 and 6 summarize the conclusions and plans for future work, respectively.

2. POSITIONING ALGORITHMS

The intelligent urban positioning system comprises four main algorithms as shown in Figure 1. The least-squares 3DMA GNSS ranging algorithm is used to initialize the likelihood-based 3DMA GNSS ranging algorithm and the shadow-matching algorithm, enabling them to use a much smaller search area than if the conventional GNSS position was used for initialization. The integration algorithms then compute a joint position solution from likelihood-based 3DMA ranging and shadow matching. Both a position-domain integration algorithm and a hypothesis-domain integration algorithm are presented. The least-squares 3DMA GNSS ranging solution is also integrated with shadow matching in the position domain to enable comparison of the new IUP algorithms with those presented in [32]. Thus, three integrated position solutions are produced altogether. The following subsections summarize each algorithm.

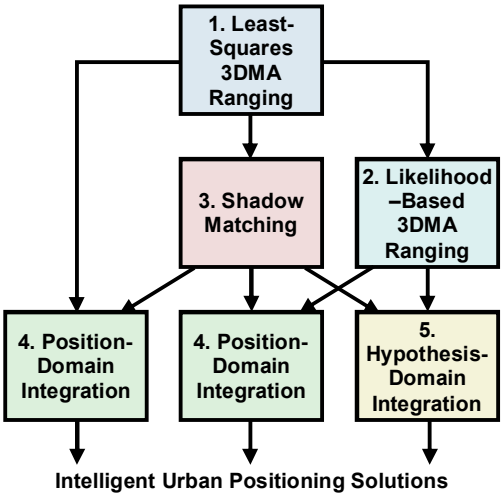

Figure 1: Intelligent urban positioning algorithm configuration

2.1. Least-Squares 3DMA GNSS Ranging

Figure 2 shows the least-squares 3DMA ranging algorithm, comprising the following six steps:

1. A search area is determined using the conventional GNSS position solution on the first iteration and the previous solution on subsequent iterations, together with an appropriate confidence interval.
2. Using 3D mapping converted to precomputed building boundaries, the proportion of the search area within which each satellite is directly visible is computed, giving the probability that the signal is direct LOS.
3. A consistency-checking process is applied to the ranging measurements, using the direct LOS probabilities from the 3D mapping.

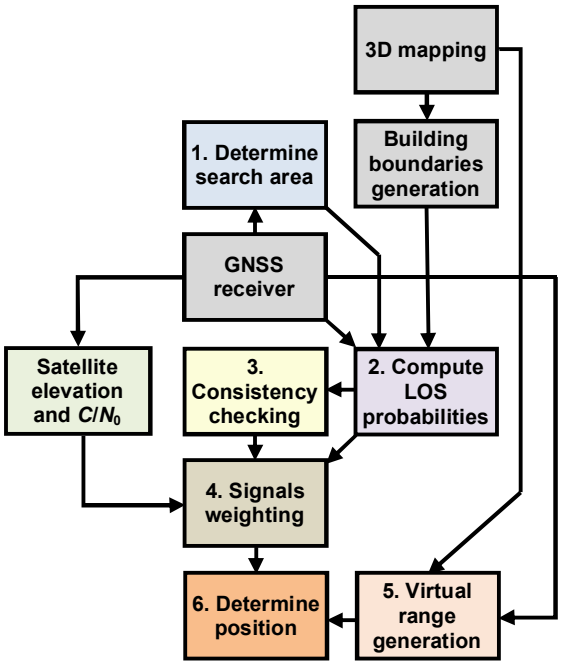

Figure 2: Least-squares 3DMA GNSS ranging algorithm block diagram (Adapted from [6]).

4. The set of signals resulting from the consistency checking process is subjected to a weighting strategy based on the previously determined LOS probabilities and carrier-power-to-noise-density ratio, C/N_0.
5. Terrain height is extracted from the 3D mapping and a virtual range measurement is generated using the position at the centre of the search area.
6. Finally, a position solution is derived from the pseudo-ranges and virtual range measurement using weighted least-squares estimation.

The algorithm is then iterated several times to improve the position solution. Full details are presented in [6] (final version) and [33] (preliminary version).

Projected coordinates (eastings and northings) are used for the 3D mapping while Cartesian ECEF coordinates are used for the least-squares position solution. Conversion between Cartesian ECEF and projected coordinates can be simplified using a nearby reference point [32].

2.2. Likelihood-based 3DMA GNSS Ranging

In likelihood-based 3DMA GNSS ranging an array of candidate position hypotheses are scored according to the correspondence between the predicted and measured pseudo-ranges. This enables different error distributions to be assumed for a given GNSS signal at different candidate positions. Thus, at positions where a signal is predicted from the 3D mapping (via precomputed building boundaries), to be NLOS, a skew normal (Gaussian) distribution is assumed, biased towards positive ranging errors. Elsewhere, a conventional symmetric normal distribution is assumed.

Terrain height aiding is inherent in generating the position hypotheses, enabling a single height to be associated with each horizontal position and thus avoiding the computational load of a 3D search area. The receiver clock bias is eliminated by differencing all pseudo-range measurements across satellites.

Other likelihood-based 3DMA GNSS ranging algorithms based on candidate position hypothesis scoring have been described in the literature. However, they differ from the approach proposed here. In [26] and [27], pseudo-ranges predicted to be NLOS are corrected using path delays predicted from the 3D mapping. This is potentially more accurate, but the path delay computation is highly computationally intensive. In [24], a least-squares position solution is computed using only those signals predicted to be direct LOS and the candidate position is then scored according to its Mahalanobis distance from the least-squares position solution.

Figure 3 shows the likelihood-based 3D-model-aided ranging algorithm, comprising the following six steps:

1. A circular search area of radius 40m is defined with its centre at the least-squares 3DMA ranging position solution. Within this search area, a grid of candidate positions is set up with a spacing of 1m.
2. For each candidate position, the satellite visibility is predicted using the building boundaries precomputed from the 3D city model. At each candidate position, the highest elevation satellite predicted to be direct LOS is selected as the reference satellite.
3. At each candidate position, the direct LOS range to each satellite is computed. Measurement innovations are then computed by subtracting the computed ranges from the measured pseudo-ranges and then differencing with respect to the reference satellite.

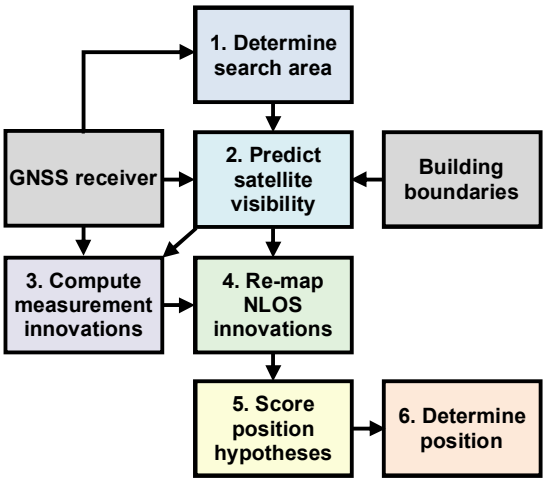

Figure 3: Likelihood-based 3DMA GNSS ranging algorithm block diagram

4. At each candidate position, the measurement innovation for each satellite predicted to be NLOS is re-mapped to a skew normal distribution.
5. A likelihood score for each candidate position, p, is computed using

$$\Lambda_{Rp} = \exp\left(-\delta\mathbf{z}_p^{\mathrm{T}}\mathbf{C}_{\delta\mathbf{z},p}^{-1}\delta\mathbf{z}_p\right), \quad (1)$$

where $\delta\mathbf{z}_p$ is the vector of measurement innovations and $\mathbf{C}_{\delta\mathbf{z},p}$ is the measurement error covariance matrix, computed using the direct-LOS-hypothesis measurement error standard deviations, which are the same for all candidate positions.

6. A position solution is derived from the scores of the candidate positions using

$$\hat{E}_R = \frac{\sum_p \Lambda_{Rp} E_p}{\sum_p \Lambda_{Rp}}, \quad \hat{N}_R = \frac{\sum_p \Lambda_{Rp} N_p}{\sum_p \Lambda_{Rp}}, \quad (2)$$

where E_p and N_p are the easting and northing coordinates of the p^{th} candidate position.

Full details of the algorithm will be presented in a forthcoming journal submission, currently under preparation.

2.3. Shadow Matching

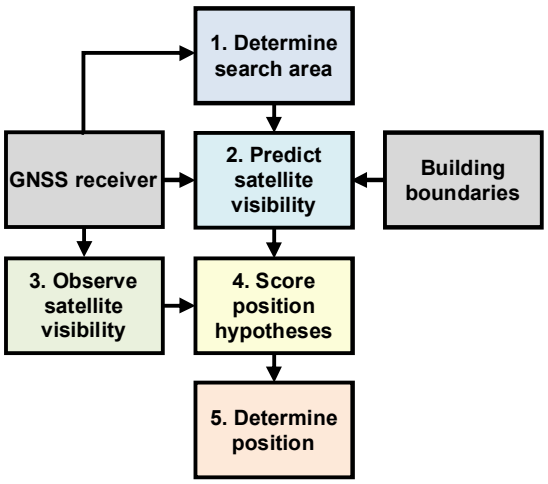

Figure 4: Shadow-matching algorithm block diagram (adapted from [20])

The shadow matching algorithm is a modified version of that presented in [16]. Figure 4 shows the algorithm, comprising the following five steps:

1. A circular search area of radius 40m is defined with its centre at the least-squares 3DMA ranging position solution. Within this search area, a grid of candidate positions is set up is set up with a spacing of 1m.
2. For each candidate position, the satellite visibility is predicted using the building boundaries precomputed from the 3D city model. If the satellite elevation is above the building boundary at the relevant azimuth, the LOS probability predicted from the building

boundary, $p(LOS|BB)$, is set to 0.85. Otherwise, it is set to 0.2. These values allow for diffraction and 3D model errors.

3. The observed satellite visibility is determined from the GNSS receiver's C/N_0 or signal to noise ratio (SNR) measurements. From these, a probability that each received signal is direct LOS, $p(LOS|SNR=s)$ is estimated using

$$p(LOS \mid SNR = s) = \begin{cases} p_{o-\min} & s < s_{\min} \\ a_2 s^2 + a_1 s + a_0 & s_{\min} < s < s_{\max} \\ p_{o-\max} & s_{\max} < s \end{cases}, \quad (3)$$

where the coefficients are listed in Table 1.

4. Each candidate position is scored according to the match between the predicted and measured satellite visibility. For a given satellite, the probability that the predicted and measured satellite visibility match is

$$P_m = \begin{array}{l} 1 - p(LOS \mid SNR = s) - p(LOS \mid BB) \\ +\, 2p(LOS \mid SNR = s)p(LOS \mid BB) \end{array} \quad (4)$$

The overall likelihood score, Λ_{Sp}, for each position, p, is then the product of the individual satellite probabilities.

5. A position solution is derived from the scores of the candidate positions using

$$\hat{E}_S = \frac{\sum_p \Lambda_{Sp} E_p}{\sum_p \Lambda_{Sp}}, \quad \hat{N}_S = \frac{\sum_p \Lambda_{Sp} N_p}{\sum_p \Lambda_{Sp}}, \quad (5)$$

where E_p and N_p are the easting and northing coordinates of the p^{th} candidate position.

Table 1: Coefficients for determining direct LOS probability from measured SNR.

Coefficient	u-blox EVK M8T	Nexus 9 tablet
$p_{o\text{-}\min}$	0.25	0.16
$s_{\min}$	23 dB-Hz	20 dB-Hz
a_0	-3.517	-0.9043
a_1	0.2411 (dB-Hz)$^{-1}$	0.0563 (dB-Hz)$^{-1}$
a_2	-0.003171 (dB-Hz)$^{-2}$	-0.00015 (dB-Hz)$^{-2}$
$p_{o\text{-}\max}$	0.89	0.94
$s_{\max}$	31 dB-Hz	35 dB-Hz

2.4. Position-Domain Integration

The position-domain integration algorithm uses the error covariance matrices of the 3DMA ranging and shadow matching position solutions to compute a weighted average of the two positions using

$$\hat{\mathbf{x}}_a^{EN} = \left(\mathbf{C}_S^{EN^{-1}} + \mathbf{C}_R^{EN^{-1}}\right)^{-1}\left(\mathbf{C}_S^{EN^{-1}}\hat{\mathbf{x}}_S^{EN} + \mathbf{C}_R^{EN^{-1}}\hat{\mathbf{x}}_R^{EN}\right), \quad (6)$$

where $\hat{\mathbf{x}}_a^{EN} = \begin{pmatrix}\hat{E}_a & \hat{N}_a\end{pmatrix}^{\mathrm{T}}$ is the integrated position solution of the user antenna, a, $\hat{\mathbf{x}}_S^{EN} = \begin{pmatrix}\hat{E}_S & \hat{N}_S\end{pmatrix}^{\mathrm{T}}$ is the shadow-matching solution, $\hat{\mathbf{x}}_R^{EN} = \begin{pmatrix}\hat{E}_R & \hat{N}_R\end{pmatrix}^{\mathrm{T}}$ is the 3DMA ranging solution, $\mathbf{C}_S^{EN}$ is the shadow-matching error covariance, and $\mathbf{C}_R^{EN}$ is the 3DMA ranging error covariance.

For least-squares 3DMA GNSS ranging, the error covariance is calculated using the following steps:

1. Compute a weighting matrix equal to the inverse of the measurement error covariance matrix, including the height aiding measurement and re-weighting from the direct LOS probabilities obtained from the 3D city model.
2. Use the least-squares measurement matrix to obtain the error covariance of the Cartesian ECEF position solution.
3. Transform the position solution error covariance matrix to the local navigation frame and extract the Easting and Northing components.

Full details of this process are presented in [32].

For shadow matching and likelihood-based 3DMA ranging, an error covariance must be extracted from a likelihood surface that is non-Gaussian and potentially multimodal. The error covariance therefore needs to be larger for multimodal distributions than it is for unimodal. The error covariance is therefore calculated using the following steps:

1. Compute an initial error covariance from the second statistical moments of the likelihood surface.
2. Determine the directions of the maximum and minimum of the error ellipse corresponding to the initial error covariance.
3. Compute the kurtosis of the likelihood surface along the maximum- and minimum-covariance directions.
4. Rescale the error ellipse using the two kurtoses.

Again, full details are presented in [32].

2.5. Hypothesis-Domain Integration

Both shadow matching and likelihood-based 3DMA ranging can produce multimodal position distributions where there is a good match between predictions and measurements in more than one part of the search area. These will typically comprise the true position hypothesis and one or more false hypotheses. In general, the true position hypothesis will be consistent across the two positioning methods whereas the false hypotheses will not be. Hypothesis-domain integration therefore helps to eliminate false position hypotheses by computing a joint ranging and shadow matching likelihood surface prior to determining a position solution. Here, it is only applied to likelihood-based 3DMA ranging.

The likelihoods are first combined using

$$\Lambda_p = \Lambda_{Rp}\Lambda_{Sp} \quad \forall p, \quad (7)$$

noting that equal weighting of the two positioning methods is assumed here.

The position solution is then obtained using

$$\hat{E}_a = \frac{\sum_p \Lambda_p E_p}{\sum_p \Lambda_p}, \quad \hat{N}_a = \frac{\sum_p \Lambda_p N_p}{\sum_p \Lambda_p}, \tag{8}$$

where E_p and N_p are the easting and northing coordinates of the p^{th} candidate position.

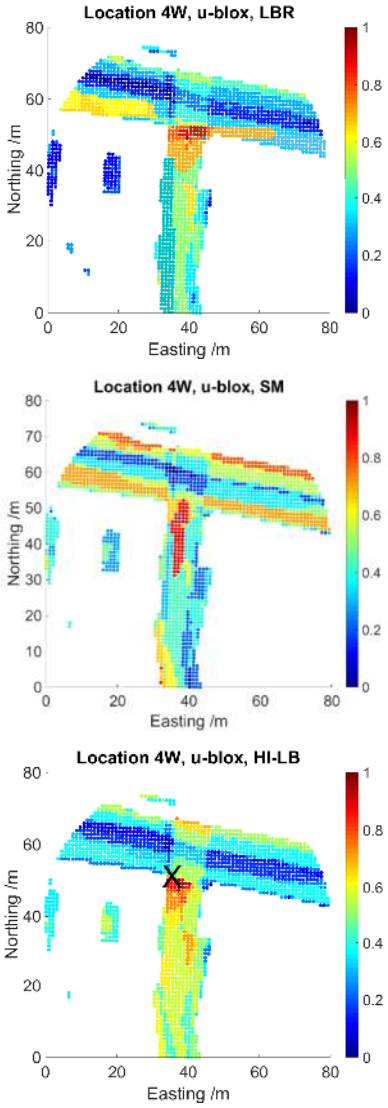

Figure 5. Normalised log-likelihoods of candidate positions at test location 4W from likelihood-based ranging (top), shadow matching (middle) and hypothesis-domain integration (bottom). The cross shows the true position. White areas are indoors

Figure 5 shows example likelihood surfaces from 3DMA ranging, shadow-matching, and the hypothesis-domain integrated solution using a u-blox GNSS receiver at test site 4W (see Section 3 below). In this case, 3DMA ranging gives a clear position solution, but this is on the wrong side of the street. The shadow matching likelihood surface has a maximum that is closer to the true position in the across-street direction, but further away in the along-street direction. There are also high-scoring areas in the next street. The integrated likelihood surface has a clear maximum that is much closer to the true position than either 3DMA ranging or shadow matching.

3. EXPERIMENTAL RESULTS

GNSS measurements, comprising GPS and GLONASS, were collected in August 2016 using a u-blox EVK M8T GNSS receiver and a HTC Nexus 9 tablet. U-blox data collection was performed by interfacing the receiver to a Raspberry Pi (via USB) for data logging, where this latter was powered by a battery pack and configured as a WiFi hotspot to which a smartphone was connected (using the mobile SSH App) to configure the system and enable data logging. Figure 6 illustrates the u-blox-based hardware.

The Nexus 9 data collection was performed using a purposely written App capturing both NMEA sentences as well as GNSS "raw data", including GNSS satellite pseudo-ranges. This latter was possible as the tablet was running the latest Android operating system, version 7.0, also known as Nougat. The tablet device is illustrated in Figure 7. The tablet's GNSS receiver and antenna are similar to those found on smartphones, so the results should be a good prediction of the performance of smartphones compatible with the Nougat GNSS interface.

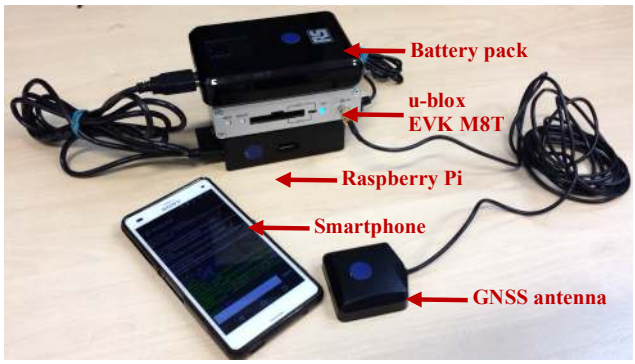

Figure 6. U-blox EVK M8T-based data logging hardware.

Figure 7. Nexus 9 tablet running Android 7.0 (Nougat) Operating System and a dedicated App for raw GNSS data logging.

Two rounds of data collection were performed using both devices at two different sites: at 18 locations in the City of London and 10 locations in Canary Wharf. Figures 8 –11 illustrate these sites. The City of London area is typical of a traditional European city with narrow streets and buildings packed close together. The Canary Wharf area is representative of a modern city environment, found more commonly in North American and East Asian cities. The streets are wider and the buildings taller with more space between them. There is also a greater ratio of glass and steel to brick and stone than in the City of London district.

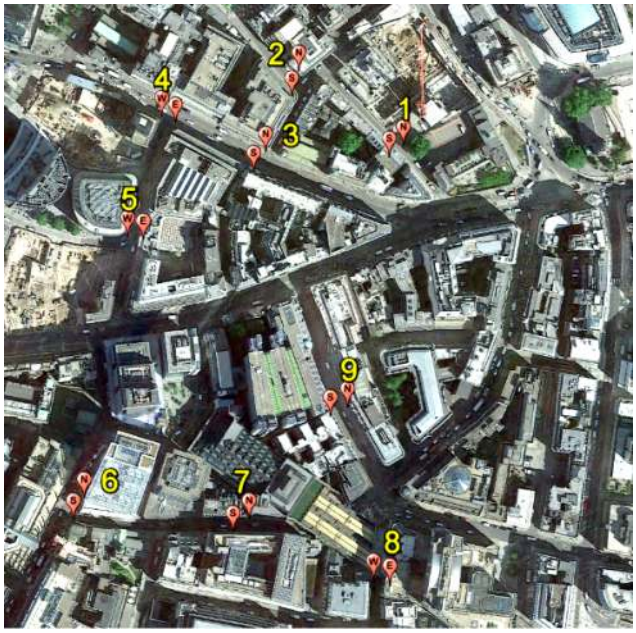

Figure 8. Data collection sites in the City of London (GoogleTM earth).

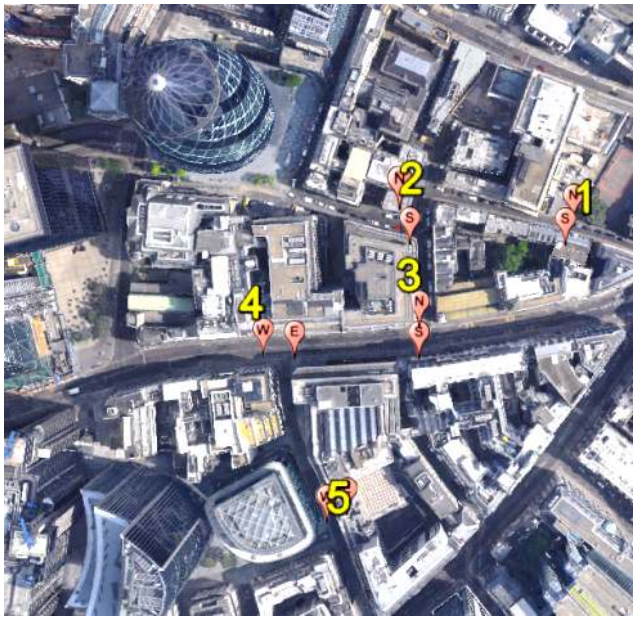

Figure 9. Part of data collection sites in the City of London – 3D view (GoogleTM earth).

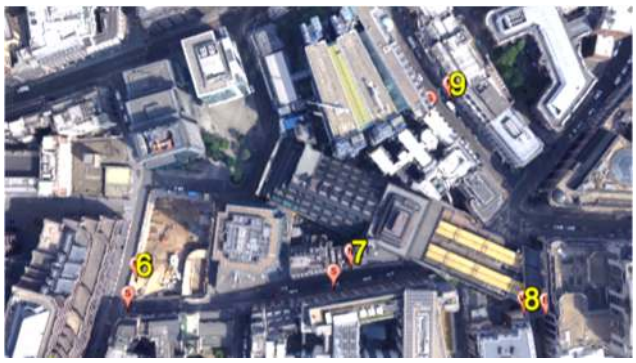

Figure 10. Part of data collection sites in the City of London – 3D view (GoogleTM earth).

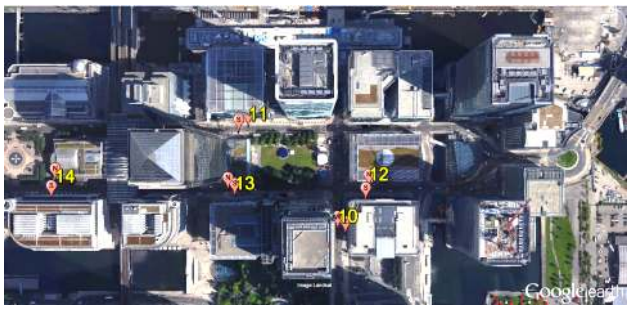

Figure 11. Data collection sites in the Canary Wharf area - London – 3D view (GoogleTM earth).

All tablet data collection was collocated with the corresponding u-blox data collection. The sites were paired with data collected on opposite sides of the street on the edge of the footpath next to the road. The truth was established to decimeter-level accuracy using a 3D city model to identify landmarks and tape measure to measure the relative position of the user from those identified landmarks. The two rounds of data at each site were separated by approximately 2 hours, ensuring that the satellite positions in the two datasets were independent. The first dataset was used for calibrating the shadow-matching algorithm (Section 2.3) for the tablet and u-blox antenna and receiver characteristics using the procedure described in [16]; the coefficients are presented in Table 1. The second dataset was then used for testing the positioning algorithms. 4 minutes of data were collected at each site on each round.

A 3D city model of the area, from Ordnance Survey (OS), was used to generate the building boundary data used for the subsequent analysis. The model is stored in the Virtual Reality Modelling Language (VRML) format. Figure 12 and 13 illustrate the 3D model used in this study.

Tables 2–7 in the appendix present the RMS along-street, across-street and horizontal (2D) position errors for each test site and positioning method using the u-blox EVK M8T receiver and antenna. Figures 14 and 15 depict the combined RMS errors across the City of London and Canary Wharf sites, respectively.

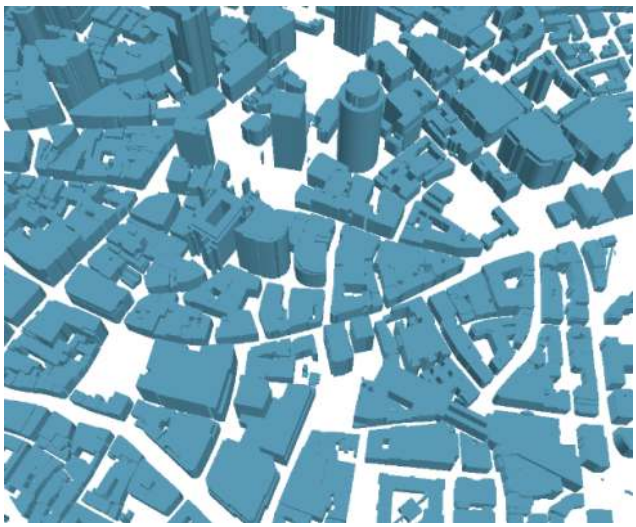

Figure 12. The 3D model of City of London used in the experiments.

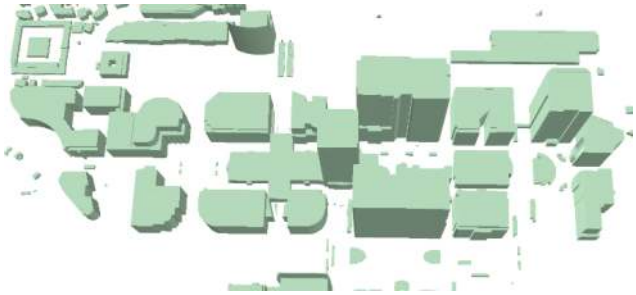

Figure 13. The 3D model of Canary Wharf used in the experiments.

Comparing the ranging-based positioning results, it can be seen that the position errors using least-squares 3DMA ranging are between a third and a half of those using conventional least-squares GNSS positioning. In the City of London, the likelihood-based 3DMA ranging algorithm is almost twice as accurate as the least-squares 3DMA ranging algorithm in the along-street direction, but only slightly better in the across-street direction. In the Canary Wharf, the likelihood-based 3DMA ranging algorithm is more than twice as accurate as the least-squares 3DMA ranging algorithm in both directions.

In the City of London area, shadow matching in the across-street direction is more than 10 times as accurate as conventional GNSS positioning and nearly 3 times as accurate as likelihood-based 3DMA ranging. In the along-street direction, shadow matching is slightly more accurate than conventional GNSS, but much less accurate than either 3DMA ranging algorithm. The same pattern is seen in the Canary Wharf results, but is much less pronounced. In the across-street direction, shadow matching is only 30% more accurate than likelihood-based 3DMA ranging. In the along-street direction, likelihood-based 3DMA ranging is more than twice as accurate as shadow matching, but least-squares 3DMA ranging is slightly less accurate.

The reason for this difference in performance between the City of London and Canary Wharf sites is the building geometry. There is a much greater difference between along-street and across-street geometry in the City of London sites than in the Canary Wharf sites.

Examining the overall horizontal position errors in the City of London, the two 3DMA ranging algorithms and shadow matching exhibit similar accuracies, however the integrated position solution is more than twice as accurate as that of any of the individual positioning algorithms. Thus, there is a clear advantage in using the intelligent urban position approach. With the Canary Wharf data, likelihood-based 3DMA ranging is 30% more accurate than shadow matching, while the hypothesis-domain integrated solution is 17% more accurate than likelihood-based 3DMA ranging alone. In general, hypothesis-domain integration leads to a 5–10% more accurate position solution than position-domain integration.

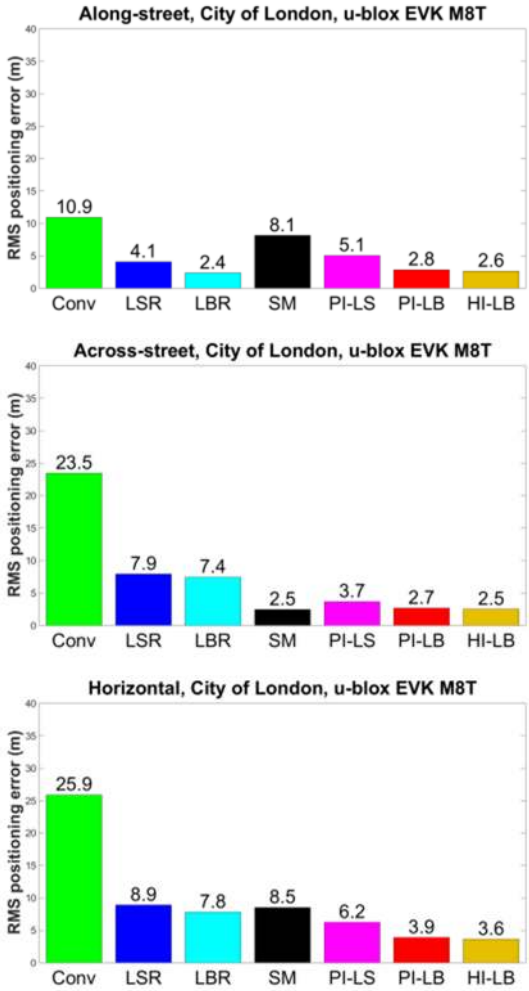

Figure 14. u-blox City of London along-street, across-street and overall horizontal RMS positioning.

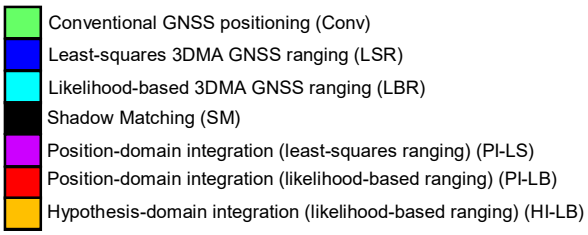

Legend for Figures 14 – 16.

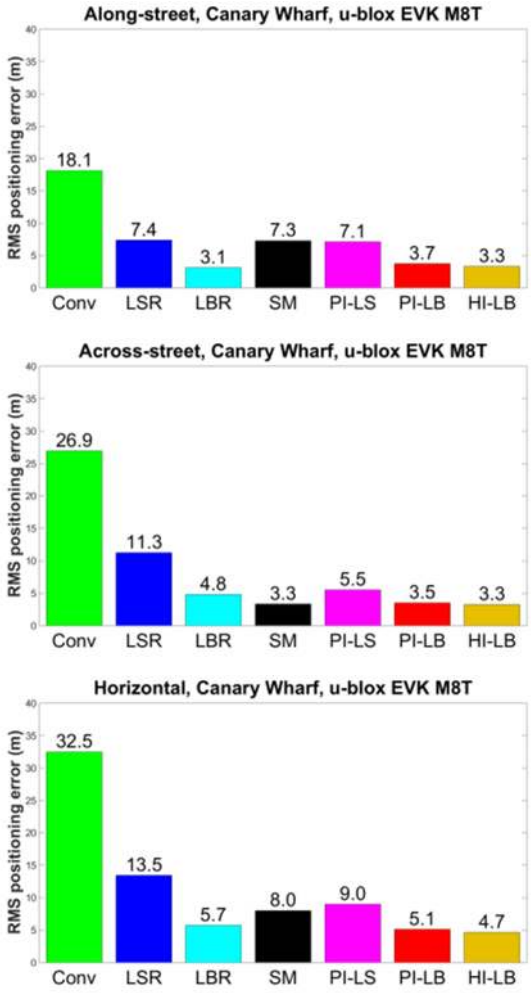

Figure 15. u-blox Canary Wharf along-street, across-street and overall horizontal RMS positioning error.

Figure 16 shows the combined RMS errors across all sites for each positioning method. It can be clearly seen that likelihood-based 3DMA ranging outperforms least-squares 3DMA ranging and that the integrated solution is much more accurate than 3DMA ranging or shadow matching alone. Comparing the best solution, hypothesis-domain integration, with conventional GNSS positioning, it can be seen that intelligent urban positioning is a factor of 7.1 more accurate using the u-blox receiver and antenna.

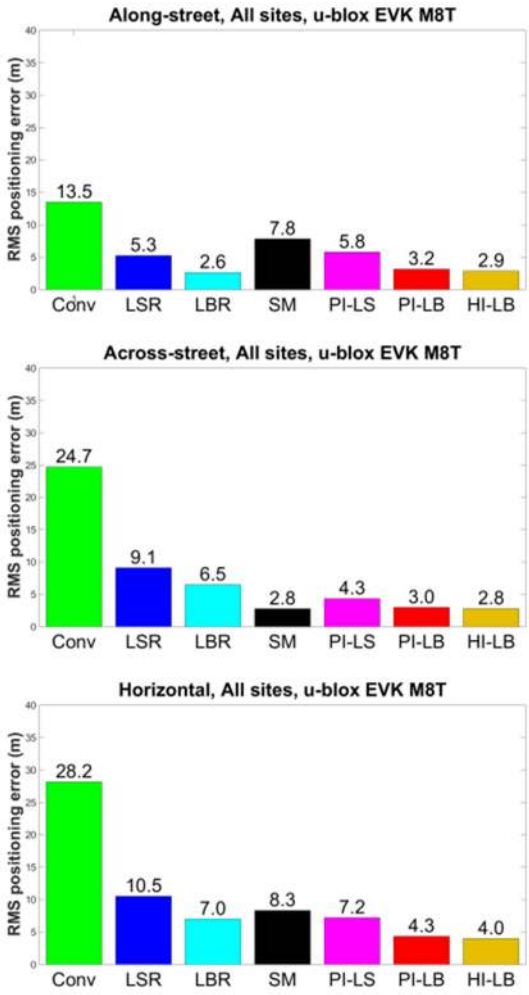

Figure 16. u-blox all sites across-street and overall horizontal RMS positioning error.

Tables 8–13 in the appendix present the RMS along-street, across-street and horizontal (2D) position errors for each test site and positioning method using the HTC Nexus 9 tablet running Android 7.0 (Nougat). Figures 17 and 18 depict the combined RMS errors across the City of London and Canary Wharf sites, respectively.

It can immediately be seen that the Nexus 9 results are not as good as the u-blox results, with conventional GNSS positioning affected least and shadow matching affected most. This is due to the inferior characteristics of a tablet (or smartphone) antenna, compared to the u-blox antenna. As the tablet antenna has no polarization discrimination, the direct LOS ranging measurements are subject to greater multipath interference and it is more difficult to distinguish LOS from NLOS signals using SNR measurements. Conventional positioning is least affected because it is dominated by the NLOS ranging errors that 3DMA positioning helps to minimize; these are not affected by the antenna design.

Comparing the different positioning methods and the different environments, the same trends as in the u-blox results are seen, but are less pronounced. With the City of London data, the hypothesis-domain integrated solution is 37% more accurate than the best individual algorithm, likelihood-based 3DMA GNSS. With the Canary Wharf data, the integrated solution is only 15% more accurate than likelihood-based 3DMA GNSS.

Figure 19 shows the combined RMS errors across all sites for each positioning method. Again, likelihood-based 3DMA ranging outperforms least-squares 3DMA ranging and that the integrated solution is more accurate than 3DMA ranging or shadow matching alone. Comparing the best solution, hypothesis-domain integration, with conventional GNSS positioning, it can be seen that intelligent urban positioning is a factor of 4.7 more accurate using the Nexus 9 tablet.

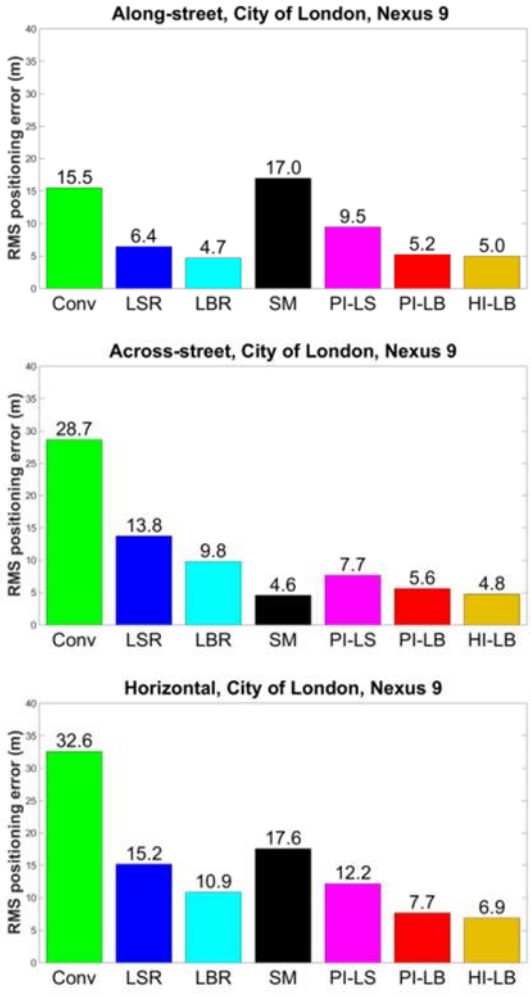

Figure 17. Nexus 9 City of London along-street, across-street and overall horizontal RMS positioning error.

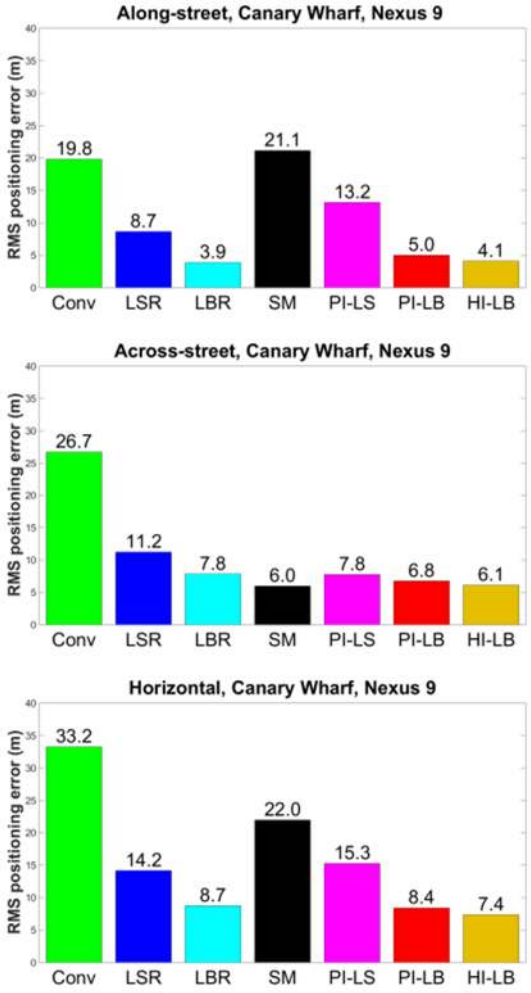

Figure 18. Nexus 9 Canary Wharf along-street, across-street and overall horizontal RMS positioning error.

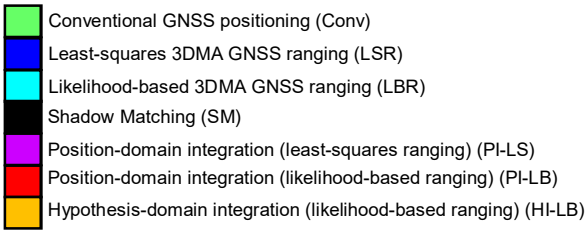

Legend for Figures 17 – 19.

An interesting area to focus on is site 8E. The conventional GNSS RMS positioning error is 63.8m using the u-blox receiver and 75.9m using the tablet. However, the IUP RMS errors are 7.7m with the u-blox receiver and 8.7m with the tablet, a factor of 8–9 improvement in both cases. Figure 20 shows the position errors for each epoch from the u-blox data. The along-street direction was roughly north-south so the conventional GNSS position error is largest in the across-street direction. Thus, intelligent urban positioning was still effective even in the most challenging environments.

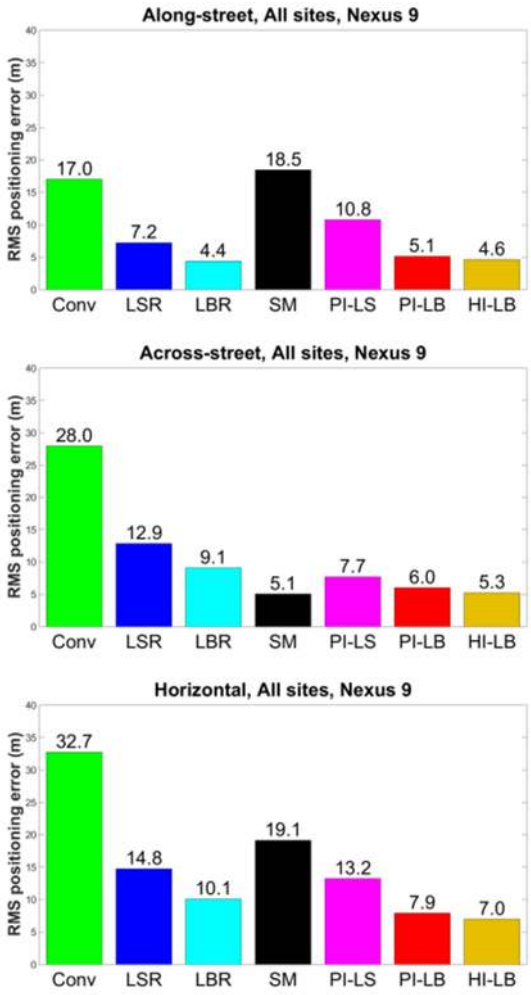

Figure 19. Nexus 9 all sites along-street, across-street and overall horizontal RMS positioning error.

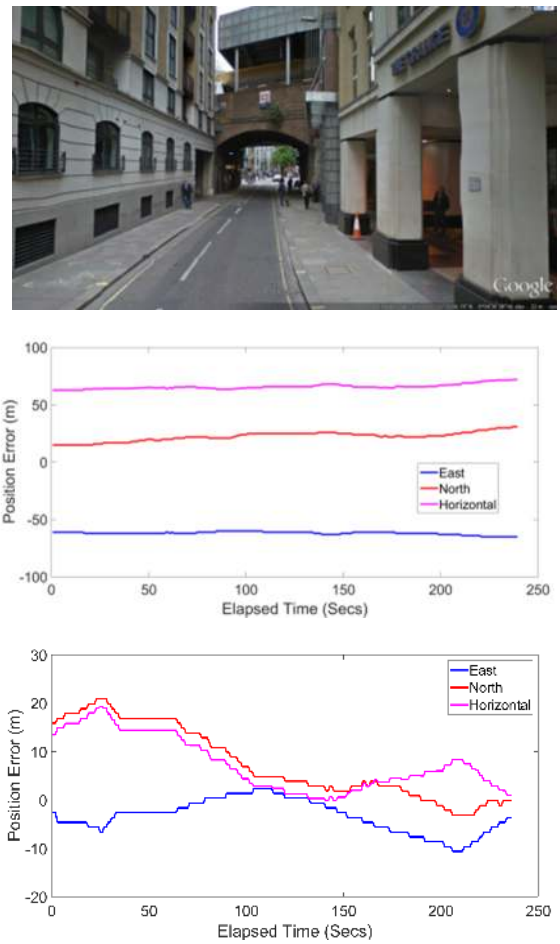

Figure 20. U-blox receiver position error at location 8E – street view 8E (top), conventional GNSS ranging positioning (middle) and hypothesis-domain integration (bottom).

4. PRACTICAL IMPLEMENTATION

There are four ways in which 3D-mapping-aided GNSS, including the intelligent urban positioning algorithms presented here, could be implemented in a practical system:

- Post-processing of recorded data is suited to data collection applications such as mapping, and monitoring the movement of people, animals or vehicles for research purposes.
- Real-time implementation on a remote server is suited to location-based services requiring a one-time position fix and to tracking applications with long update intervals.
- Real-time implementation on a mobile device using pre-loaded mapping data is suited to professional navigation and continuous tracking applications within a limited area.
- Real-time implementation on a mobile device using streamed mapping data is suited to consumer and professional navigation and continuous tracking applications.

A practical real-time implementation of any 3DMA GNSS system requires the following [34]:

- Real-time access to GNSS pseudo-range and SNR or C/N_0 measurements;
- Computationally efficient positioning algorithms;
- Access to 3D mapping data;
- A means of distributing the GNSS measurements and mapping data to the positioning algorithms.

Survey receivers have always provided the necessary GNSS measurements, but are not practical for most 3DMA GNSS applications. Obtaining them from consumer receivers has historically been problematic. However, today, receivers such as the u-blox M8T provide pseudo-range and SNR measurements from all GNSS constellations and a new interface provides access to this data through the application programming interface (API) on smartphones and tablets running the Android Nougat operating system that have a compatible GNSS chipset.

By using building boundaries instead of accessing the 3D mapping directly, the intelligent urban positioning algorithms presented here are able to run quickly. On a DELL Precision M2800 laptop computer (running the Microsoft Windows 7 operating system equipped with 16GB RAM and a quad-core processor with a 2.5GHz base frequency) it takes about 233 ms to compute a position solution from one epoch of GNSS measurement data. A new smartphone or tablet has 25–75% as much processing power as this laptop. Therefore, these algorithms should easily be able to run at 1 Hz on a mobile device.

Highly detailed 3D mapping is expensive. However, simple block models, known as level of detail (LOD) 1, are sufficient for most 3D-mapping-aided GNSS implementations. Examples are shown in Figures 12 and 13. Open Street Map provides freely available building mapping for the world's major cities and many other places, much of it in 3D. Data is also available from national mapping agencies. Although coverage is not universal, it tends to be available in the dense urban areas where it is most needed.

This leaves data distribution. For server-based positioning, existing assisted GNSS interfaces can be used to transmit pseudo-range and SNR measurements from mobile devices to a server.

To run the positioning algorithms on a mobile device, mapping data is required. The terrain height data are easiest to handle. A 5m grid spacing is sufficient, corresponding to 40,000 points per km^2. 12 bits is sufficient to describe the relative height of a point within a tile, while 4 bytes are needed for the height of each tile's origin with respect to the datum. Thus, about 60 kB per km^2 is needed, so 1GB of storage could accommodate about 17,000 km^2 of data, much more with compression. Thus, this data could be pre-loaded in a mobile device.

Building boundaries require a lot more data. To a 1° precision, about 300 bytes are needed per building boundary. Assuming about half the space in a city is outdoor (building boundaries are not required for indoor locations), a 100×100m tile would require 1.5MB of data without compression, so 1GB of storage would only accommodate about 7 km^2 of data, maybe 70 km^2 with compression. Thus, pre-loading is only practical for users that operate within a relatively small area.

To stream building boundary data, only the search area is needed, which should be no bigger than 100×100m, considering only outdoor locations. Furthermore, only azimuths corresponding to the current set of GNSS satellites are needed, which reduces the amount of data required to 90kB without compression. Less than a kilobyte of terrain height data would be needed. 3G mobile download speeds are higher than 500 kB/s (4 Mbit/s). Therefore, streaming is easily practical and substantial data buffering could be accommodated to bridge gaps in communications coverage. Note that for continuous positioning, successive search areas will considerably overlap so it is not necessary to transmit a full set of mapping data at every epoch.

5. CONCLUSIONS

A full implementation of the intelligent urban positioning 3D-mapping-aided GNSS concept has been presented, including a new likelihood-based 3DMA ranging algorithm and a hypothesis-based algorithm for integrating ranging with shadow matching. Both new algorithms have been shown to perform better than their predecessors.

The IUP algorithms were tested using data recorded using a u-blox EVK M8T consumer-grade GNSS receiver and a Nexus 9 tablet at 28 locations across two districts of London, representative of both traditional and modern dense urban environments. The Nexus 9 tablet used the Android Nougat GNSS receiver interface, so is representative of future smartphones. With the u-blox receiver, the single-epoch RMS horizontal (i.e., 2D) error across all sites was 4.0 m using the IUP algorithms, compared to 28.2 m for conventional positioning, a factor of 7.1 improvement. Using the Nexus tablet, the IUP RMS error was 7.0 m, compared to 32.7 m for conventional GNSS positioning, a factor of 4.7 improvement.

An analysis of processing and data requirments has shown that intelligent urban positioning is practical to implement in real-time on a mobile device or a server.

6. FUTURE WORK

The following work is planned for the next year:

- Tests with a geodetic-grade GNSS receiver to determine the performance achievable with high-quality user equipment.
- Development of a real-time demonstration system using the Raspberry Pi and u-blox EVK 8MT platform.
- Extensive testing to quantify the effects of different error sources on both shadow matching and 3DMA GNSS ranging.
- Develop environmental context determination algorithms to determine from the GNSS measurement data when the receiver is in an environment where it can benefit from intelligent urban positioning, building on the work presented in [35].
- Development of a multi-epoch version of the intelligent urban positioning algorithms presented here for both static and dynamic applications.

Longer term aspirations include:

- Implementation of outlier detection to compensate for out-of-date mapping and transient effects, such as passing buses.

- Computation of real-time performance metrics to provide rudimentary integrity.
- Integration of 3DMA GNSS with inertial sensors and other navigation technologies for added robustness.
- Further development of the shadow-matching algorithms as discussed in [20].

ACKNOWLEDGEMENTS

This work is funded by the Engineering and Physical Sciences Research Council (EPSRC) project EP/L018446/1, *Intelligent Positioning in Cities using GNSS and Enhanced 3D Mapping*. The project is also supported by Ordnance Survey, u-blox and the Royal National Institute for Blind People.

The authors would also like to thank Han Gao of UCL for assisting with the experimental data collection.

REFERENCES

[1] Groves, P. D., "GNSS Solutions: Multipath vs. NLOS signals. How Does Non-Line-of-Sight Reception Differ From Multipath Interference," *Inside GNSS Magazine*, Nov/Dec 2013, pp. 40-42, 63.

[2] Groves, P. D., *Principles of GNSS, inertial, and multi-sensor integrated navigation systems*, Second Edition, Artech House, 2013.

[3] Bhuiyan M. Z. H. and Lohan, E. S., "Multipath Mitigation Techniques for Satellite-Based Positioning Applications," in Jin, S. (Ed.) *Global Navigation Satellite Systems: Signal, Theory and Applications*, InTech, 2012, pp. 405-426

[4] Groves, P. D. and Jiang, Z., "Height Aiding, C/N0 Weighting and Consistency Checking for GNSS NLOS and Multipath Mitigation in Urban Areas". *Journal of Navigation*, 66, 2013, 653–669. Also available from http://discovery.ucl.ac.uk/.

[5] Amt, J. R. and Raquet, J. F., "Positioning for Range-Based Land Navigation Systems Using Surface Topography," *Proc. ION GNSS* 2006, Fort Worth, TX, 1494–1505.

[6] Adjrad, M., and Groves, P. D., "Enhancing Least Squares GNSS Positioning with 3D Mapping without Accurate Prior Knowledge," Accepted for publication in *NAVIGATION*, 2016.

[7] Bradbury, J., Ziebart, M., Cross, P. A., Boulton, P. & Read, A., "Code Multipath Modelling in the Urban Environment Using Large Virtual Reality City Models: Determining the Local Environment". *Journal of Navigation,* 60(1), 2007, 95-105.

[8] Suh, Y. and Shibasaki, R.., "Evaluation of satellite-based navigation services in complex urban environments using a three-dimensional GIS". *IEICE Transactions on Communications,* E90-B**,** 2007, 1816-1825.

[9] Wang, L., Groves, P. D. and Ziebart, M. K., "Multi-Constellation GNSS Performance Evaluation for Urban Canyons Using Large Virtual Reality City Models," *Journal of Navigation*, 65(3), 2012, 459–476. Also available from http://discovery.ucl.ac.uk/.

[10] Groves, P. D., "Shadow Matching: A New GNSS Positioning Technique for Urban Canyons". *Journal of Navigation*, 64(3), 2011, 417-430. Also available from http://discovery.ucl.ac.uk/.

[11] Ben-Moshe, B., et al., "Improving Accuracy of GNSS Devices in Urban Canyons". *23rd Canadian Conference on Computational Geometry*, 2011.

[12] Wang, L., Groves, P. D. and Ziebart, M. K., "GNSS Shadow Matching Using A 3D Model of London". *European Navigation Conference*, London, 2011. Also available from http://discovery.ucl.ac.uk/.

[13] Suzuki, T., and Kubo, N., "GNSS Positioning with Multipath Simulation using 3D Surface Model in Urban Canyon". *ION GNSS* 2012, Nashville, TN.

[14] Wang, L., Groves, P. D. and Ziebart, M. K., "GNSS Shadow Matching: Improving Urban Positioning Accuracy Using a 3D City Model with Optimized Visibility Prediction Scoring". *NAVIGATION*, 60(3), 2013, 195–207. (First published at *ION GNSS,* 2012, Nashville, TN). Also available from http://discovery.ucl.ac.uk/.

[15] Isaacs, J. T., Irish, A. T., et al., "Bayesian localization and mapping using GNSS SNR measurements". *IEEE/ION PLANS* 2014. Monterey, California.

[16] Wang, L., Groves, P. D. and Ziebart, M. K., "Smartphone Shadow Matching for Better Cross-street GNSS Positioning in Urban Environments". *Journal of Navigation*, 68(3), 2015, 411–433. Also available from http://discovery.ucl.ac.uk/.

[17] Wang, L., *Investigation of Shadow Matching for GNSS Positioning in Urban Canyons*, PhD Thesis, University College London, 2015. Available from http://discovery.ucl.ac.uk/.

[18] Yozevitch, R. and Ben-Moshe, B., "A Robust Shadow Matching Algorithm for GNSS Positioning," *NAVIGATION*, 62(2), 2015, 95–109.

[19] Wang, L., Groves, P. D. and Ziebart, M. K., "Urban Positioning on a Smartphone: Real-time Shadow Matching Using GNSS and 3D City Models". *ION GNSS+* 2013, Nashville, Tennessee. AND *Inside GNSS*, Nov/Dec 2013, 44–56. Also available from http://discovery.ucl.ac.uk/.

[20] Groves, P. D., Wang, L., Adjrad, M., and Ellul, C., "GNSS Shadow Matching: The Challenges Ahead". *ION GNSS+* 2015, Tampa, Florida. Also available from http://discovery.ucl.ac.uk/.

[21] Obst, M., S. Bauer, and G. Wanielik, "Urban Multipath Detection and mitigation with Dynamic

3D Maps for Reliable Land Vehicle Localization," *IEEE/ION PLANS* 2012.

[22] Bourdeau, A. and Sahmoudi, M., "Tight Integration of GNSS and a 3D City Model for Robust Positioning in Urban Canyons". *ION GNSS* 2012, Nashville, Tennessee.

[23] Peyraud, S., et al., "About Non-Line-Of-Sight Satellite Detection and Exclusion in a 3D Map-Aided Localization Algorithm," *Sensors*, Vol. 13, 2013, pp. 829-847.

[24] Suzuki, T., "Integration of GNSS Positioning and 3D Map using Particle Filter" *ION GNSS*+ 2016, Portland, Oregon.

[25] Suzuki, T., and Kubo N., "Correcting GNSS Multipath Errors Using a 3D Surface Model and Particle Filter," *ION GNSS*+ 2013, Nashville, TN.

[26] Kumar, R. and Petovello, M, G., "A Novel GNSS Positioning Technique for Improved Accuracy in Urban Canyon Scenarios using 3D City Model", *ION GNSS*+ 2014, Tampa, FL.

[27] Hsu, L.-T., Gu, Y., and Kamijo, S., "3D building model-based pedestrian positioning method using GPS/GLOANSS/QZSS and its reliability calculation", *GPS Solutions*, 2015, doi 10.1007/s10291-015-0451-7.

[28] Kumar, R. and Petovello, M, G., "Sensitivity Analysis of 3D Building Model-assisted Snapshot Positioning", *ION GNSS*+ 2016, Portland, Oregon.

[29] Betaille, D., et al., "A New Modeling Based on Urban Trenches to Improve GNSS Positioning Quality of Service in Cities". *IEEE Intelligent Transportation Systems Magazine*, 5(3), 2013, 59–70.

[30] Ng, Y. and Gao, G. X., "Direct Positioning Utilizing Non Line of Sight (NLOS) GPS Signals", *ION GNSS*+ 2016, Portland, Oregon.

[31] Groves, P. D., Jiang, Z., Wang, L. and Ziebart, M., "Intelligent Urban Positioning using Multi-Constellation GNSS with 3D Mapping and NLOS Signal Detection". *ION GNSS* 2012. Nashville, Tennessee. Also available from http://discovery.ucl.ac.uk/.

[32] Adjrad, M., and Groves, P. D., "Intelligent Urban Positioning: Integration of Shadow Matching with 3D-Model-Aided GNSS Ranging," *Submitted for journal publication*, 2016. Please email the authors to obtain a copy before publication.

[33] Adjrad, M., and Groves, P. D., "Enhancing Conventional GNSS Positioning with 3D Mapping without Accurate Prior Knowledge". *ION GNSS*+ 2015, Tampa, Florida. Also available from http://discovery.ucl.ac.uk/.

[34] Groves, P. D., "It's Time for 3D-Mapping-Aided GNSS". *Inside GNSS*, Sep/Oct 2016.

[35] Gao, H., and Groves, P. D., "Context Determination for Adaptive Navigation using Multiple Sensors on a Smartphone". *ION GNSS*+ 2016, Portland, Oregon.

APPENDIX

Table 2. Details of along-street positioning results using u-blox EVK M8T receiver – The City of London site.

Algorithm	Conventional GNSS	Least-squares 3DMA GNSS ranging	Likelihood-based 3DMA GNSS ranging	Shadow matching	Position-domain integration (least-squares ranging)	Position-domain integration (likelihood-based ranging)	Hypothesis-domain integration (likelihood-based ranging)
Location	Along-street RMS error (m)	Along-street RMS error (m)	Along-street RMS error (m)	Along-street RMS error (m)	Along-street RMS error (m)	Along-street RMS error (m)	Along-street RMS error (m)
1N	10.8	3.6	2	8.5	4.8	2.9	2.3
1S	11.4	3.5	1.9	9.4	3.9	2.3	2.1
2N	6.5	2.8	1.2	5.6	3.7	1.5	1.3
2S	6.6	2.8	1.2	10.1	3.3	1.7	1.4
3N	10.3	2.9	1.3	8.6	3.5	1.6	1.4
3S	7.7	3.1	1.5	9.8	4	1.9	1.7
4W	6.7	2.6	1	4.8	3.2	1.2	1.1
4E	6.4	2.8	1.2	5.7	3.6	1.5	1.4
5W	5.6	2.5	0.9	6.3	4.2	1.3	1.1
5E	5.9	3.2	1.6	7.3	4.5	2.2	1.8
6N	10.2	3.5	1.9	6.5	4.7	2.1	2
6S	9.4	3.5	1.9	14	5.2	2.4	2.2
7N	11	3.6	2	5.9	4.5	2.2	2.1
7S	11.8	5.8	4.2	8.1	6.9	4.4	4.3
8W	25.4	7.9	6.3	11.6	8.6	6.5	6.5
8E	23.1	8.5	6.9	11.8	10	7.2	7

9N	15.8	4.8	3.2	6	5.5	3.4	3.2
9S	11.9	6	2.4	6.6	6.8	4.8	4.5

Table 3. Details of across-street positioning results using u-blox EVK M8T receiver – The City of London site.

Algorithm	Conventional GNSS	Least-squares 3DMA GNSS ranging	Likelihood-based 3DMA GNSS ranging	Shadow matching	Position-domain integration (least-squares ranging)	Position-domain integration (likelihood-based ranging)	Hypothesis-domain integration (likelihood-based ranging)
Location	Across-street RMS error (m)	Across -street RMS error (m)	Across -street RMS error (m)	Across-street RMS error (m)	Across-street RMS error (m)	Across-street RMS error (m)	Across-street RMS error (m)
1N	17.8	6.5	4.9	2.2	2.9	2.4	2.3
1S	18.9	5.9	5.9	1.6	2.8	1.7	1.7
2N	23.6	6.7	6.7	2.7	3.5	2.7	2.7
2S	16.5	5.9	5.9	2	3	2.2	2.1
3N	22.8	5.7	5.7	2.1	3.4	2.4	2.3
3S	18.5	6.9	6.9	2	2.7	2.6	2.2
4W	19.9	5.7	5.7	2.7	3.4	2.8	2.8
4E	17.4	5.6	5.6	3	3.3	3.2	3.1
5W	11.3	4.9	3.9	2.2	2.9	2.4	2.3
5E	9.5	4.9	2.9	2.3	3	2.3	2.3
6N	22.1	7.9	7.9	1.6	2.2	1.9	1.8
6S	15.4	5.9	5.9	1.4	2.3	1.7	1.6
7N	23.6	7.7	7.7	2.2	2.6	2.6	2.4
7S	18.1	8.9	6.9	2.3	3.9	3.4	2.5
8W	66.6	18.9	18.9	1.5	6.2	2	1.6
8E	59.5	21.9	21.9	3.2	7.1	3.3	3.1
9N	27.9	7.1	7.1	3	4.9	3.1	3.1
9S	13	5.5	3.5	6.2	6	5.5	5.5

Table 4. Details of horizontal positioning results using u-blox EVK M8T receiver – The City of London site.

Algorithm	Conventional GNSS	Least-squares 3DMA GNSS ranging	Likelihood-based 3DMA GNSS ranging	Shadow matching	Position-domain integration (least-squares ranging)	Position-domain integration (likelihood-based ranging)	Hypothesis-domain integration (likelihood-based ranging)
Location	Horizontal RMS error (m)	Horizontal RMS error (m)	Horizontal RMS error (m)	Horizontal RMS error (m)	Horizontal RMS error (m)	Horizontal RMS error (m)	Horizontal RMS error (m)
1N	20.8	7.4	5.3	8.8	5.6	3.8	3.3
1S	22.1	6.9	6.2	9.5	4.8	2.9	2.7
2N	24.5	7.3	6.8	6.2	5.1	3.1	3
2S	17.8	6.5	6	10.3	4.5	2.8	2.5
3N	25	6.4	5.8	8.9	4.9	2.9	2.7
3S	20	7.6	7.1	10	4.8	3.2	2.8
4W	21	6.3	5.8	5.5	4.7	3	3
4E	18.5	6.3	5.7	6.4	4.9	3.5	3.4
5W	12.6	5.5	4	6.7	5.1	2.7	2.5
5E	11.2	5.9	3.3	7.7	5.4	3.2	2.9
6N	24.3	8.6	8.1	6.7	5.2	2.8	2.7
6S	18	6.9	6.2	14.1	5.7	2.9	2.7
7N	26	8.5	8	6.3	5.2	3.4	3.2
7S	21.6	10.6	8.1	8.4	7.9	5.6	5
8W	71.3	20.5	19.9	11.7	10.6	6.8	6.7
8E	63.8	23.5	23	12.2	12.3	7.9	7.7
9N	32.1	8.6	7.8	6.7	7.4	4.6	4.5
9S	17.6	8.1	4.2	9.1	9.1	7.3	7.1

Table 5. Details of along-street positioning results using u-blox EVK M8T receiver – Canary Wharf site.

Algorithm	Conventional GNSS	Least-squares 3DMA GNSS ranging	Likelihood-based 3DMA GNSS ranging	Shadow matching	Position-domain integration (least-squares ranging)	Position-domain integration (likelihood-based ranging)	Hypothesis-domain integration (likelihood-based ranging)
Location	Along-street RMS error (m)	Along-street RMS error (m)	Along-street RMS error (m)	Along-street RMS error (m)	Along-street RMS error (m)	Along-street RMS error (m)	Along-street RMS error (m)
10W	14.8	6.1	2.6	9.2	7	3.5	2.7
10E	16.4	6.7	2.8	9.8	7.4	3.9	3
11S	16.7	6.8	2.9	5.3	6	3.5	3.2
11N	16.4	6.7	2.8	6.1	6.5	3.3	3
12S	15.6	6.3	2.7	6.7	6.6	3.4	2.9
12N	15.9	6.5	2.7	7.7	7	3.1	2.8
13S	19	7.7	3.3	6.3	7.2	3.9	3.6
13N	21.8	8.8	3.8	8.5	8.7	4.3	4.1
14S	22.8	9.3	3.9	6.3	7.5	4.4	4
14N	21.9	8.9	3.8	6.9	7.3	4.1	3.9

Table 6. Details of across-street positioning results using u-blox EVK M8T receiver – Canary Wharf site.

Algorithm	Conventional GNSS	Least-squares 3DMA GNSS ranging	Likelihood-based 3DMA GNSS ranging	Shadow matching	Position-domain integration (least-squares ranging)	Position-domain integration (likelihood-based ranging)	Hypothesis-domain integration (likelihood-based ranging)
Location	Across-street RMS error (m)	Across-street RMS error (m)	Across-street RMS error (m)	Across-street RMS error (m)	Across-street RMS error (m)	Across-street RMS error (m)	Across-street RMS error (m)
10W	27.8	11.6	4.9	3.1	5.2	3.5	3.2
10E	28.9	12.1	5.1	1.9	6.3	2.4	2.2
11S	29.9	12.5	5.3	3.4	4.9	3.8	3.6
11N	27.4	11.5	4.9	3.6	5.7	4.1	3.7
12S	21.3	8.9	3.8	2.7	4.5	3.2	2.8
12N	19.5	8.1	3.5	3	5.5	3.3	3.2
13S	29.6	12.3	5.3	2.5	4.2	2.9	2.7
13N	28.1	11.7	5	2.8	5.1	3.2	2.9
14S	33.9	14.2	6.1	3.9	5.9	4.1	4
14N	23	9.6	4.2	6.5	7.8	4.6	4.3

Table 7. Details of horizontal positioning results using u-blox EVK M8T receiver – Canary Wharf site.

Algorithm	Conventional GNSS	Least-squares 3DMA GNSS ranging	Likelihood-based 3DMA GNSS ranging	Shadow matching	Position-domain integration (least-squares ranging)	Position-domain integration (likelihood-based ranging)	Hypothesis-domain integration (likelihood-based ranging)
Location	Horizontal RMS error (m)	Horizontal RMS error (m)	Horizontal RMS error (m)	Horizontal RMS error (m)	Horizontal RMS error (m)	Horizontal RMS error (m)	Horizontal RMS error (m)
10W	31.5	13.1	5.5	9.7	8.7	4.9	4.2
10E	33.2	13.8	5.8	10	9.7	4.6	3.7
11S	34.2	14.2	6	6.3	7.7	5.2	4.8
11N	31.9	13.3	5.6	7.1	8.6	5.3	4.8
12S	26.4	10.9	4.7	7.2	8	4.7	4
12N	25.2	10.4	4.4	8.3	8.9	4.5	4.3
13S	35.2	14.5	6.2	6.8	8.3	4.9	4.5
13N	35.6	14.6	6.3	8.9	10.1	5.4	5
14S	40.9	17	7.2	7.4	9.5	6	5.7
14N	31.8	13.1	5.7	9.5	10.7	6.2	5.8

Table 8. Details of along-street positioning results using Nexus 9 tablet – The City of London site.

Algorithm	Conventional GNSS	Least-squares 3DMA GNSS ranging	Likelihood-based 3DMA GNSS ranging	Shadow matching	Position-domain integration (least-squares ranging)	Position-domain integration (likelihood-based ranging)	Hypothesis-domain integration (likelihood-based ranging)
Location	Along-street RMS error (m)	Along-street RMS error (m)	Along-street RMS error (m)	Along-street RMS error (m)	Along-street RMS error (m)	Along-street RMS error (m)	Along-street RMS error (m)
1N	12	5.1	3.6	10.1	7.3	4	3.7
1S	12.5	5.3	3.8	10.6	8.1	4.1	3.9
2N	10.1	4.2	3.1	12	5.9	3.5	3.3
2S	8.6	3.6	2.6	12.3	6.3	2.9	2.8
3N	12.9	5.3	3.9	14.5	7.9	4.3	4
3S	11.5	4.8	3.5	13.1	8.1	4	3.7
4W	8.5	3.5	2.6	10	6.9	3.2	2.8
4E	6.9	2.9	2.1	8	4.7	2.9	2.5
5W	30.1	12.5	9.1	33	15.9	10.5	10.1
5E	28.5	11.9	8.6	33.9	17.3	9.1	8.8
6N	12.5	5.2	3.8	15.2	9.9	4.2	4.1
6S	10	4.2	3.1	15.3	6.7	3.5	3.7
7N	14.1	5.8	4.2	18.1	8.8	4.3	4.5
7S	15.9	6.6	4.8	20.4	10.5	5.7	4.9
8W	30.2	12.5	9.1	34.7	19.2	10.3	9.6
8E	26	10.8	7.8	30.6	13.5	8	7.9
9N	16	6.7	4.8	6.7	6.7	5	4.9
9S	12.7	5.2	3.8	7.1	6.7	4.4	3.9

Table 9. Details of across-street positioning results using Nexus 9 tablet – The City of London site.

Algorithm	Conventional GNSS	Least-squares 3DMA GNSS ranging	Likelihood-based 3DMA GNSS ranging	Shadow matching	Position-domain integration (least-squares ranging)	Position-domain integration (likelihood-based ranging)	Hypothesis-domain integration (likelihood-based ranging)
Location	Across-street RMS error (m)	Across-street RMS error (m)	Across-street RMS error (m)	Across-street RMS error (m)	Across-street RMS error (m)	Across-street RMS error (m)	Across-street RMS error (m)
1N	18.2	8.7	6.1	3	4.2	4.1	3.2
1S	19.5	9.3	6.5	2.1	4.6	2.9	2.5
2N	28	13.4	9.4	5.9	7.8	7	6
2S	18	8.6	6	4.8	5.7	5.5	5
3N	23.1	11	7.7	3.7	7.7	4.7	3.8
3S	19.5	9.3	6.5	4.2	8.3	5.5	4.4
4W	18.5	8.8	6.2	4.6	5.5	5.1	4.7
4E	14.2	6.8	6.6	6	6.5	6.4	6.1
5W	41	20	13.6	5.1	10.3	6.8	5.3
5E	37.2	17.7	12.4	8.8	12.5	10.3	9.1
6N	23.4	11.2	7.8	5.7	6.7	6.7	6
6S	15.2	7.3	5.1	3.9	4.8	4.4	4.2
7N	24.3	11.6	8.1	2.7	6.6	4.3	2.8
7S	20.1	9.6	6.7	4.5	7.5	5.4	4.6
8W	80	38.1	26.6	3.3	10.2	4.3	3.4
8E	71.3	34	23.7	3.4	12.8	5.9	3.6
9N	30.3	14.5	10.1	3.6	9.2	4.8	3.9
9S	14	7.8	7.3	6.9	7.2	7.2	7.3

Table 10. Details of horizontal positioning results using Nexus 9 tablet – The City of London site.

Algorithm	Conventional GNSS	Least-squares 3DMA GNSS ranging	Likelihood-based 3DMA GNSS ranging	Shadow matching	Position-domain integration (least-squares ranging)	Position-domain integration (likelihood-based ranging)	Hypothesis-domain integration (likelihood-based ranging)
Location	Horizontal RMS error (m)	Horizontal RMS error (m)	Horizontal RMS error (m)	Horizontal RMS error (m)	Horizontal RMS error (m)	Horizontal RMS error (m)	Horizontal RMS error (m)
1N	21.8	10.1	7.1	10.5	8.4	5.7	4.9
1S	23.2	10.7	7.5	10.8	9.3	5	4.6
2N	29.8	14	9.9	13.4	9.8	7.8	6.8
2S	19.9	9.3	6.5	13.2	8.5	6.2	5.7
3N	26.5	12.2	8.6	15	11	6.4	5.5
3S	22.6	10.5	7.4	13.8	11.6	6.8	5.7
4W	20.4	9.5	6.7	11	8.8	6	5.5
4E	15.8	7.4	6.9	10	8	7	6.6
5W	50.9	23.6	16.4	33.4	18.9	12.5	11.4
5E	46.9	21.3	15.1	35	21.3	13.7	12.7
6N	26.5	12.3	8.7	16.2	12	7.9	7.3
6S	18.2	8.4	6	15.8	8.2	5.6	5.6
7N	28.1	13	9.1	18.3	11	6.1	5.3
7S	25.6	11.6	8.2	20.9	12.9	7.9	6.7
8W	85.5	40.1	28.1	34.9	21.7	11.2	10.2
8E	75.9	35.7	25	30.8	18.6	9.9	8.7
9N	34.3	16	11.2	7.6	11.4	6.9	6.3
9S	18.9	9.4	8.2	9.9	9.8	8.4	8.3

Table 11. Details of along-street positioning results using Nexus 9 tablet – Canary Wharf site.

Algorithm	Conventional GNSS	Least-squares 3DMA GNSS ranging	Likelihood-based 3DMA GNSS ranging	Shadow matching	Position-domain integration (least-squares ranging)	Position-domain integration (likelihood-based ranging)	Hypothesis-domain integration (likelihood-based ranging)
Location	Along-street RMS error (m)	Along-street RMS error (m)	Along-street RMS error (m)	Along-street RMS error (m)	Along-street RMS error (m)	Along-street RMS error (m)	Along-street RMS error (m)
10W	16.5	7.2	3.1	17.8	11.7	4.9	3.5
10E	19.5	8.5	3.7	20.3	12.3	4.8	4
11S	18.9	8.3	5.6	19.5	14.5	6.7	5.8
11N	17	7.4	3.2	18.5	10.3	4.3	3.4
12S	16.4	7.2	3.1	17.9	9.2	4.9	3.3
12N	17.3	7.6	2.3	19	11.9	3.8	2.5
13S	20.7	9	3.9	22.5	14.6	4.6	4.1
13N	23.9	10.4	4.5	25.3	17.2	5.6	4.7
14S	24.2	10.6	4.7	26.1	13.3	5.3	4.9
14N	23.6	10.3	4.5	24.5	16.5	5.1	4.8

Table 12. Details of across-street positioning results using Nexus 9 tablet – Canary Wharf site.

Algorithm	Conventional GNSS	Least-squares 3DMA GNSS ranging	Likelihood-based 3DMA GNSS ranging	Shadow matching	Position-domain integration (least-squares ranging)	Position-domain integration (likelihood-based ranging)	Hypothesis-domain integration (likelihood-based ranging)
Location	Across-street RMS error (m)	Across-street RMS error (m)	Across-street RMS error (m)	Across-street RMS error (m)	Across-street RMS error (m)	Across-street RMS error (m)	Across-street RMS error (m)
10W	20.3	8.7	6.9	5.4	6.6	6.2	5.5
10E	18.9	7.8	8	6.3	7.1	7.1	6.4
11S	44	18.8	8.4	5.9	8.8	6.3	6.1
11N	38.9	16.6	12.8	10.3	12.3	11	10.4
12S	26.6	10.5	7.8	6.4	7.7	7.1	6.5
12N	19.9	7.6	6.9	4.1	5.2	4.9	4.3
13S	26.1	11.2	6	3.9	6.6	5.1	4.1
13N	22.5	9.6	6.9	5.4	7	6	5.5
14S	29.6	12.6	8	6.7	8.9	7.6	6.8
14N	20.2	8.9	6.7	5.3	7.3	6.3	5.5

Table 13. Details of horizontal positioning results using Nexus 9 tablet – Canary Wharf site.

Algorithm	Conventional GNSS	Least-squares 3DMA GNSS ranging	Likelihood-based 3DMA GNSS ranging	Shadow matching	Position-domain integration (least-squares ranging)	Position-domain integration (likelihood-based ranging)	Hypothesis-domain integration (likelihood-based ranging)
Location	Horizontal RMS error (m)	Horizontal RMS error (m)	Horizontal RMS error (m)	Horizontal RMS error (m)	Horizontal RMS error (m)	Horizontal RMS error (m)	Horizontal RMS error (m)
10W	26.2	11.3	7.6	18.6	13.4	7.9	6.5
10E	27.2	11.5	8.8	21.3	14.2	8.6	7.5
11S	47.9	20.6	10.1	20.4	17	9.2	8.4
11N	42.5	18.2	13.2	21.2	16	11.8	10.9
12S	31.2	12.7	8.4	19	12	8.6	7.3
12N	26.4	10.7	7.3	19.4	13	6.2	5
13S	33.3	14.4	7.2	22.8	16	6.9	5.8
13N	32.8	14.2	8.2	25.9	18.6	8.2	7.2
14S	38.2	16.5	9.3	26.9	16	9.3	8.4
14N	31.1	13.6	8.1	25.1	18	8.1	7.3